Inorganic Chemistry
Article

Inorg. Chem. **2010**, *49*, 2057–2067 **2057**
DOI: 10.1021/ic9016504

Axial Ligand Orientations in a Distorted Porphyrin Macrocycle: Synthesis, Structure, and Properties of Low-Spin Bis(imidazole)iron(III) and Iron(II) Porphyrinates†

Ranjan Patra, Arvind Chaudhary, Sudip Kumar Ghosh, and Sankar Prasad Rath*

Department of Chemistry, Indian Institute of Technology Kanpur, Kanpur 208016, India

Received August 18, 2009

We have reported here, for the first time, the parallel and perpendicular orientation preferences of two planar and unhindered imidazoles as axial ligands (L) while coordinated toward iron(III) and iron(II) porphyrins, respectively, in a nonplanar porphyrinic environment. The synthesis and characterization of low-spin Fe^{III}(*tn*-OEP)$(L)_2\cdot ClO_4$ and Fe^{II}(*tn*-OEP)$(L)_2$ are reported. Fe^{III}(*tn*-OEP)$(L)_2\cdot ClO_4$ shows rhombic electron paramagnetic resonance (EPR) spectra (at 77 K) in both solid and solution phases that are very characteristic for low-spin ($S = {}^1/_2$) iron porphyrins with two axial imidazole ligands aligned parallel to each other. Single-point energy calculation is also performed on Fe^{III}(*tn*-OEP)$(1\text{-MeIm})_2^+$ using density functional theory (DFT), which shows that the relative parallel orientations of two 1-MeIm are more stable than the perpendicular orientations. X-ray structures of Fe^{II}(*tn*-OEP)$(1\text{-MeIm})_2$ and Fe^{II}(*tn*-OEP)$(1\text{-MeIm})_2\cdot$THF are reported that demonstrate, for the first time, the near-perpendicular axial ligand orientation (80.9 and 89.8°, respectively) for iron(II) porphyrins in a distorted macrocyclic environment. Even starting from parallel axial orientations of 1-MeIm, geometry optimization using DFT converged well to the perpendicular axial alignment with a 82.54° dihedral angle, which is in close agreement with experiment. This is in sharp contrast to all earlier reports, in which sterically crowded imidazole (such as 2-MeIm) or a nearly planar porphyrin core with a "picket fence" environment that restricts the rotation of the axial ligands is required for perpendicular orientation. Electrochemical data obtained from a cyclic voltammetric study for Fe^{II}(*tn*-OEP)$(L)_2$ reveal one-electron oxidation at very high positive potential, which readily explains why the complexes are so stable in air. Bulk oxidation of Fe^{II}(*tn*-OEP)$(1\text{-MeIm})_2$ at a constant potential of 0.69 V in dichloromethane with 0.1 M tetrabutylammonium perchlorate as the supporting electrolyte generates Fe^{III}(*tn*-OEP)$(1\text{-MeIm})_2\cdot ClO_4$, which has the same EPR spectrum and which upon reduction at 0.29 V regenerates Fe^{II}(*tn*-OEP)$(1\text{-MeIm})_2$ again. Thus, we have demonstrated here, for the first time, that iron(II) and iron(III) porphyrinates with two planar and unhindered axial imidazoles have different orientation preferences in a nonplanar porphyrinic environment.

Introduction

Porphyrins and metalloporphyrins are conformationally flexible, and multiple macrocycle conformations have been observed crystallographically.[1−9] The heme macrocycle displays a range of distorted nonplanar shapes, which are presumably caused by different protein environments surrounding the heme. This presumption is based on evidence showing that the isolated heme group is nearly planar in solution environments and thus external forces must be

† Dedicated to Prof. Animesh Chakravorty on the occasion of his 75th birthday.

*To whom correspondence should be addressed. E-mail: sprath@iitk.ac.in.

(1) (a) Senge, M. O. In *The Porphyrin Handbook*; Kadish, K. M., Smith, K. M., Guilard, R., Eds.; Academic Press: San Diego, 2000; Vol. *1*, p 239. (b) Senge, M. O. *Chem. Commun.* **2006**, 243.

(2) (a) Shelnutt, J. A. In *The Porphyrin Handbook*; Kadish, K. M., Smith, K. M., Guilard, R., Eds.; Academic Press: New York, 2000; Vol. *7*, p 167. (b) Shelnutt, J. A.; Song, X.-Z.; Ma, J.-G.; Jia, S.-L.; Jentzen, W.; Medforth, C. J. *Chem. Soc. Rev* **1998**, *27*, 31.

(3) Scheidt, W. R. In *The Porphyrin Handbook*; Kadishi, K. M., Smith, K. M., Guilard, R., Eds.; Academic Press: San Diego, 2000; Vol. *3*, p 49.

(4) (a) Walker, F. A. *Chem. Rev.* **2004**, *104*, 589. (b) Walker, F. A. *Coord. Chem. Rev.* **1999**, *185−186*, 471.

(5) (a) Nakamura, M.; Ohgo, Y.; Ikezaki, A. *J. Inorg. Biochem.* **2008**, *102*, 433. (b) Nakamura, M. *Coord. Chem. Rev.* **2006**, *250*, 2271.

(6) (a) Cheng, R.-J.; Wang, Y.-K.; Chen, P.-Y.; Han, Y.-P.; Chang, C.-C. *Chem. Commun.* **2005**, 1312. (b) Cheng, R.-J; Chen, P.-Y.; Lovell, T.; Liu, T.; Noodleman, L.; Case, D. A. *J. Am. Chem. Soc.* **2003**, *125*, 6774.

(7) (a) Schünemann, V.; Gerdan, M.; Trautwein, A. X.; Haoudi, N.; Mandon, D.; Fischer, J.; Weiss, R.; Tabard, A.; Guilard, R. *Angew. Chem., Int. Ed.* **1999**, *38*, 3181. (b) Renner, M. W.; Barkigia, K. M.; Zhang, Y.; Medforth, C. J.; Smith, K. M.; Fajer, J. *J. Am. Chem. Soc.* **1994**, *116*, 8582.

(8) (a) Ohgo, Y.; Hoshino, A.; Okamura, T.; Uekusa, H.; Hashizume, D.; Ikezaki, A.; Nakamura, M. *Inorg. Chem.* **2007**, *46*, 8193. (b) Shao, J.; Steene, E.; Hoffman, B. M.; Ghosh, A. *Eur. J. Inorg. Chem.* **2005**, 1609. (c) Hoshino, A.; Ohgo, Y.; Nakamura, M. *Inorg. Chem.* **2005**, *44*, 7333. (d) Zakharieva, O.; Schunemann, V.; Gerdan, M.; Licoccia, S.; Cai, S.; Walker, F. A.; Trautwein, A. X. *J. Am. Chem. Soc.* **2002**, *124*, 6636.

(9) (a) Patra, R.; Chaudhury, A.; Ghosh, S. K.; Rath, S. P. *Inorg. Chem.* **2008**, *47*, 8324. (b) Ghosh, S. K.; Patra, R.; Rath, S. P. *Inorg. Chem.* **2008**, *47*, 9848. (c) Patra, R.; Rath, S. P. *Inorg. Chem. Commun.* **2009**, 515. (d) Patra, R.; Bhowmik, S.; Ghosh, S. K.; Rath, S. P. *Eur. J. Inorg. Chem.* **2009**, 654. (e) Ghosh, S. K.; Patra, R.; Rath, S. P. *Inorg. Chem.* **2008**, *47*, 10196.

Published on Web 02/03/2010

applied to cause significant nonplanar distortion.[10−12] It is believed that conformational control of the porphyrin macrocycle by the protein side chains can account, in part, for the various functions of chemically similar tetrapyrrole pigments found in nature and thus become an attractive subject to investigate the relationship between the ligand distortion and the properties of the metal center in porphyrin complexes.

Bis(histidine)-coordinated heme centers are involved in electron transfer in a number of cytochrome-containing systems including complexes II−IV of inner mitochondrial membranes.[3−5] It is believed that the arrangement of the axial ligands plays an important role in defining the spectroscopic properties and possibly also the reduction potentials of these heme centers. In the protein structures, two limiting orientations of the axial ligand planes have been implemented in the structures of the cytochromes: the imidazole planes are oriented nearly parallel to each other (cytochromes b_5,[13] three of the heme centers of cytochromes c_3,[14−16] the *b* hemes of sulfite oxidase[17] and flavocytochrome b_2,[18] and the heme *a* of cytochrome oxidase[19]), while one of the four heme groups in cytochrome c_3 from *Desulfovibrio vulgaris* has two histidine ligands in nearly perpendicular arrangement. Other hemoproteins found spectroscopically to have perpendicular axial orientations include the *b* hemes of mitochondrial complex III (also known as cytochrome bc_1[20]), the *b* hemes of cytochrome b_6f of chloroplasts, one of the *c*-type hemes of cytochrome c_3,[21] and the *c*-type heme of cytochrome c'' of *Methylophilus methylotrophus*.[22] Depending on the character of the electronic ground state, these complexes with parallel and perpendicular orientations of the axial ligands have different spectroscopic properties. Model systems have been great aids in correlating the structure of heme centers with their spectroscopic properties. It would be interesting to investigate the axial ligand orientations on the nonplanar porphyrinic environment in order to understand the effect of similar distortions observed in various heme proteins.

The influence of the interaction of axially coordinated ligands with a simple iron porphyrin core (planar porphyrin without substituents) on the orientation of axial ligands was also studied before by quantum chemical calculations. Density functional theory (DFT) calculations on $Fe^{II}(por)(Im)_2$ and $Fe^{III}(por)(Im)_2^+$ (por = porphyrin; Im = imidazole) showed that there is no difference in the preference for parallel or orthogonal orientations of imidazoles for both iron(II) and iron(III) complexes because they almost have the same energy.[23,24] This is also in agreement with the experimental data:[25−29] for model hemes with planar porphyrins that do not possess bulky substituents, practically no barrier of rotation was found for axial imidazole ligands. In cytochromes, however, free rotation of the axial ligands is precluded because of the protein environment around the molecule. In the present work, we elucidate the effect of ring deformation on the orientations of imidazoles as axial ligands.

The macrocycles can be distorted via the introduction of sterically demanding substituents in the porphyrin periphery. This objective has been achieved successfully by taking 2,3,7,8,12,13,17,18-octaethyl-5,10,15,20-tetranitroporphyrins (*tn*-H_2OEP)[30] as porphyrin macrocycles in which the presence of four electron-withdrawing bulky nitro groups at the meso positions severely distorts the porphyrin geometry. We have presented earlier a family of five- and six-coordinated high-spin iron(III) porphyrins Fe^{III}(*tn*-OEP)Cl, Fe^{III}(*tn*-OEP)(MeOH)Cl, and Fe^{III}(*tn*-OEP)$(OH_2)_2\cdot ClO_4$ in a highly saddle-distorted macrocyclic environment that enable us to scrutinize the effects of axial-ligand coordination and macrocycle deformations on metal ion displacement.[9a] It has also been suggested that the displacements of iron in proteins are a consequence of nonequivalent axial coordination as well as protein-induced deformation at the heme. We have reported here, for the first time, the parallel and perpendicular orientation preferences of two planar and unhindered imidazoles as axial ligands (L) while coordinated toward iron(III) and iron(II) porphyrins, respectively, in a nonplanar porphyrinic environment. The synthesis, structure, and properties of all of the molecules are reported here.

Results and Discussion

The free ligand (*tn*-H_2OEP) has been synthesized via demetalation of zinc tetranitrooctaethylporphyrin as reported previously,[30] and the oxo-bridged dimer $[Fe^{III}$(*tn*-OEP)$]_2$O was prepared as before.[9d] Scheme 1 shows the synthesis and structures of all of the molecules reported in the

(10) (a) Kratky, C.; Waditschatka, R.; Angst, C.; Johansen, J.; Plaquevent, J. C.; Schreiber, J.; Eschenmoser, A. *Helv. Chim. Acta* **1982**, *68*, 1312. (b) Waditschatka, R.; Kratky, C.; Jaun, B.; Heinzer, J.; Eschenmoser, A. *J. Chem. Soc., Chem. Commun.* **1985**, 1604. (c) Geno, M. K.; Halpern, J. *J. Am. Chem. Soc.* **1987**, *109*, 1238. (d) Furenlid, L. R.; Renner, M. W.; Smith, K. M.; Fajer, J. *J. Am. Chem. Soc.* **1990**, *112*, 1634.
(11) Anderson, K. K.; Hobbs, J. D.; Luo, L.; Stanley, K. D.; Quirke, J. M. E.; Shelnutt, J. A. *J. Am. Chem. Soc.* **1993**, *115*, 12346.
(12) (a) Berry, E. A; Walker, F. A. *J. Biol. Inorg. Chem.* **2008**, *13*, 481. (b) Rakic, A. A.; Medakovic, V. B.; Zaric, S. D. *J. Inorg. Biochem.* **2006**, *100*, 133.
(13) Mathews, F. S.; Czerwinski, E. W.; Argos, P. In *The Porphyrins*; Dolphin, D., Ed.; Academic Press: New York, 1979; Vol. *VII*, p 108.
(14) Pierrot, M.; Haser, R.; Frey, M.; Payan, F.; Astier, J.-P. *J. Biol. Chem.* **1982**, *257*, 14341.
(15) Higuchi, Y.; Kusunoki, M.; Matsuura, Y.; Yasuoka, N.; Kakudo, M. *J. Mol. Biol.* **1984**, *172*, 109.
(16) Czjzek, M.; Guerlesquin, F.; Bruschi, M.; Haser, R. *Structure* **1996**, *4*, 395.
(17) Kipke, C. A.; Cusanovich, M. A.; Tollin, G.; Sunde, R. A.; Enemark, J. H. *Biochemistry* **1988**, *27*, 2918.
(18) (a) Xia, Z.-X.; Shamala, N.; Bethge, P. H.; Lim, L. W.; Bellamy, H. D.; Xuong, N. H.; Lederer, F.; Mathews, F. S. *Proc. Natl. Acad. Sci. U.S.A.* **1987**, *84*, 2629. (b) Dubois, J.; Chapman, S. K.; Mathews, F. S.; Reid, G. A.; Lederer, F. *Biochemistry* **1990**, *29*, 6393.
(19) Iwata, S.; Ostermeier, C.; Ludwig, B.; Michel, H. *Nature* (*London*) **1995**, *376*, 660.
(20) (a) Salerno, J. C. *J. Biol. Chem.* **1984**, *259*, 2331. (b) Tsai, A.-L.; Palmer, G. *Biochim. Biophys. Acta* **1982**, *681*, 484. (c) Tsai, A.-L.; Palmer, G. *Biochim. Biophys. Acta* **1983**, *722*, 349.
(21) Pierrot, M.; Haser, R.; Frey, M.; Payan, F.; Astier, J.-P. *J. Biol. Chem.* **1982**, *257*, 14341.
(22) (a) Berry, M. J.; George, S. J.; Thomson, A. J.; Santos, H.; Turner, D. L. *Biochem. J.* **1990**, *270*, 413. (b) Costa, H. S.; Santos, H.; Turner, D. L.; Xavier, A. V. *Eur. J. Biochem.* **1992**, *208*, 427. (c) Costa, H. S.; Santos, H.; Turner, D. L. *Eur. J. Biochem.* **1993**, *215*, 817.
(23) Medakovic, V.; Zaric, S. D. *Inorg. Chim. Acta* **2003**, *349*, 1.
(24) Ghosh, A.; Gonzales, E.; Vangberg, T. *J. Phys. Chem. B* **1999**, *103*, 1363.
(25) Shokhirev, N. V.; Shokhireva, T. K.; Polam, J. R.; Watson, C. T.; Raffii, K.; Simons, U.; Walker, F. A. *J. Phys. Chem.* **1997**, *A101*, 2778.
(26) Grodzicki, M.; Flint, H.; Winkle, H.; Walker, F. A.; Trautwein, A. X. *J. Phys. Chem.* **1997**, *A101*, 4202.
(27) Nakamura, M.; Tajima, K.; Tada, K.; Ishizu, K.; Nakamura, N. *Inorg. Chim. Acta* **1994**, *224*, 113.
(28) Polam, J. R.; Shokhireva, T. K.; Raffi, K.; Simons, U.; Walker, F. A. *Inorg. Chim. Acta* **1997**, *263*, 109.
(29) Momot, K. I.; Walker, F. A. *J. Phys. Chem.* **1997**, *A101*, 2787.
(30) (a) Gong, L.; Dolphin, D. *Can. J. Chem.* **1985**, *63*, 401. (b) Wu, G.-Z.; Gan, W.-X.; Leung, H.-K. *J. Chem. Soc., Faraday Trans.* **1991**, *87*, 2933.

Scheme 1

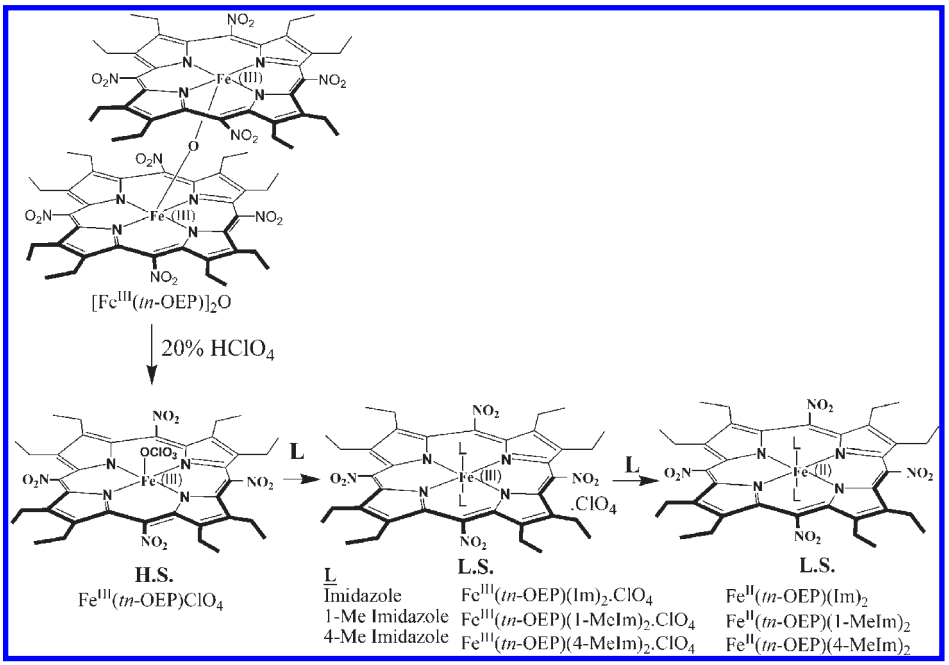

paper and their abbreviations. A dichloromethane solution of $[Fe^{III}(tn\text{-OEP})]_2O$ was shaken well with 20% aqueous $HClO_4$ and eventually changes color from its initial greenish to dark brown. The organic layer was then separated and evaporated to dryness to isolate $Fe^{III}(tn\text{-OEP})ClO_4$ in quantitative yields. The ^1H NMR spectrum (at 298 K) of the complex in $CDCl_3$ has shown only one broad methylene resonance at 40.0 ppm. The electron paramagnetic resonance (EPR) spectral measurements carried out at 77 K show similar features in both solid and solution phases. The spectra at 77 K are axially symmetric with $g_\perp = 5.90$ and $g_\parallel = 1.99$ for the frozen toluene solution and $g_\perp = 5.88$ and $g_\parallel = 2.01$ for the powder. We have reported earlier[9a] that, for high-spin $Fe^{III}(tn\text{-OEP})Cl$, the $-CH_2$ protons show only one resonance at 41.5 ppm and the molecule shows axially symmetric EPR (at 77 K) with $g_\perp = 5.98$ and $g_\parallel = 2.01$ for the frozen toluene solution and $g_\perp = 5.96$ and $g_\parallel = 2.01$ for the powder (crushed single crystals). These results provide unequivocal evidence for the high-spin (with a minor contribution from $S = {}^3/_2$) nature of $Fe^{III}(tn\text{-OEP})ClO_4$ in both solid and solution phases.

Several factors control the spin states of iron(III) porphyrin complexes. Among these, the number and nature of axial ligands are the most important factors. While most of the anionic ligands such as halides and hydroxides lead to the formation of complexes with high-spin ($S = {}^5/_2$) states, extremely weak ligands such as ClO_4^- and SbF_6^- give complexes with admixed ($S = {}^3/_2, {}^5/_2$) spin states. Fajer and co-workers have also reported[31b] that five-coordinated $Fe(OETPP)ClO_4$ is an essentially pure $S = {}^3/_2$ complex on the basis of the EPR and crystallographic studies. Our molecule $Fe^{III}(tn\text{-OEP})ClO_4$, however, shows the nearly pure high-spin nature of the molecule in both solid and solution phases. In contrast, all reported $Fe^{III}(por)ClO_4$ complexes have either mixed or intermediate spin states for iron.[31]

Because $Fe^{III}(tn\text{-OEP})ClO_4$ is prone to autoreduction upon longer exposure to a large excess of imidazoles, it is therefore treated briefly with a slight excess (2.5 equiv) of imidazoles in CH_2Cl_2, followed by the addition of *n*-hexanes that enable precipitation of the product as $Fe^{III}(tn\text{-OEP})(L)_2\cdot ClO_4$. However, the addition of a large excess of imidazoles to $Fe^{III}(tn\text{-OEP})ClO_4$ immediately forms $Fe^{III}(tn\text{-OEP})(L)_2\cdot ClO_4$ in solution, which then undergoes spontaneous autoreduction to produce air-stable $Fe^{II}(tn\text{-OEP})(L)_2$ (Scheme 1). Figure 1 shows time evaluation spectral changes of $Fe^{III}(tn\text{-OEP})ClO_4$ in the presence of an excess of 1-methylimidazoles (1-MeIm), in which peak at 377 nm corresponds to $Fe^{III}(tn\text{-OEP})ClO_4$ first transformed to the peaks at 374 and 420 nm characteristic of $Fe^{III}(tn\text{-OEP})(1\text{-MeIm})_2\cdot ClO_4$, which then upon longer exposure generates peaks at 367, 408, and 466 nm related to air-stable $Fe^{II}(tn\text{-OEP})(1\text{-MeIm})_2$. Similar observations are also obtained when other substituted imidazoles used as axial ligands form the corresponding air-stable $Fe^{II}(tn\text{-OEP})(L)_2$ in quantitative yields. In contrast, most of $Fe^{II}(por)(L)_2$ are highly air-sensitive and immediately convert to either the air-stable $Fe^{III}(por)(L)_2^+$ or the μ-oxo-bridged dimer when exposed to dioxygen.[32]

The autoreduction of iron(III) porphyrins has been reported before[33] for several potential ligands such as pyridine,

(31) (a) Sakai, T.; Ohgo, Y.; Hoshino, A.; Ikeue, T.; Saitoh, T.; Takahashi, M.; Nakamura, M. *Inorg. Chem.* **2004**, *43*, 5034. (b) Barkigia, K. M.; Renner, M. W.; Fajer, J. *J. Porphyrins Phthalocyanines* **2001**, *5*, 415. (c) Nesset, J. M.; Cai, S.; Shokhireva, T. K.; Shokhirev, N. V.; Jacobson, S. E.; Jayaraj, K.; Gold, A.; Walker, F. A. *Inorg. Chem.* **2000**, *39*, 532. (d) Reed, C. A.; Guiset, F. *J. Am. Chem. Soc.* **1996**, *118*, 3281. (e) Masuda, H.; Taga, T.; Osaki, K.; Sugimoto, H.; Yoshida, Z.; Ogoshi, H. *Inorg. Chem.* **1980**, *19*, 950. (f) Reed, C. A.; Mashiko, T.; Bentley, S. P.; Kastner, M. E.; Scheidt, W. R.; Spartalian, K.; Lang, G. *J. Am. Chem. Soc.* **1979**, *101*, 2948.

(32) (a) Kadish, K. M.; Finikova, O. S.; Espinosa, E.; Gros, C. P.; Stefano, G. D.; Cheprakov, A. V.; Beletskaya, I. P.; Guilard, R. *J. Porhphyrins Phthalocyanines* **2004**, *8*, 1062. (b) Vogler, A.; Kunkely, H.; Rethwisch, B. *Inorg. Chim. Acta* **1980**, *46*, 101.

(33) (a) Hayashi, T.; Nakashima, Y.; Ito, K.; Ikegami, T.; Aritome, I.; Aoyagi, K.; Ando, T.; Hisaeda, Y. *Inorg. Chem.* **2003**, *42*, 7345. (b) Balch, A. L.; Noll, B. C.; Olmstead, M. M.; Phillips, S. L. *Inorg. Chem.* **1996**, *35*, 6495. (c) Modi, S.; Shedbalkar, V. P.; Behere, D. V. *Inorg. Chim. Acta* **1990**, *173*, 9. (d) Srivasta, G. S.; Sawyer, D. T. *Inorg. Chem.* **1985**, *24*, 1732. (e) Shin, K.; Kramer, S. K.; Goff, H. M. *Inorg. Chem.* **1987**, *26*, 4103. (f) Del Gaudio, J.; La Mar, G. N. *J. Am. Chem. Soc.* **1978**, *100*, 1112. (g) Del Gaudio, J.; La Mar, G. N. *J. Am. Chem. Soc.* **1976**, *98*, 3014.

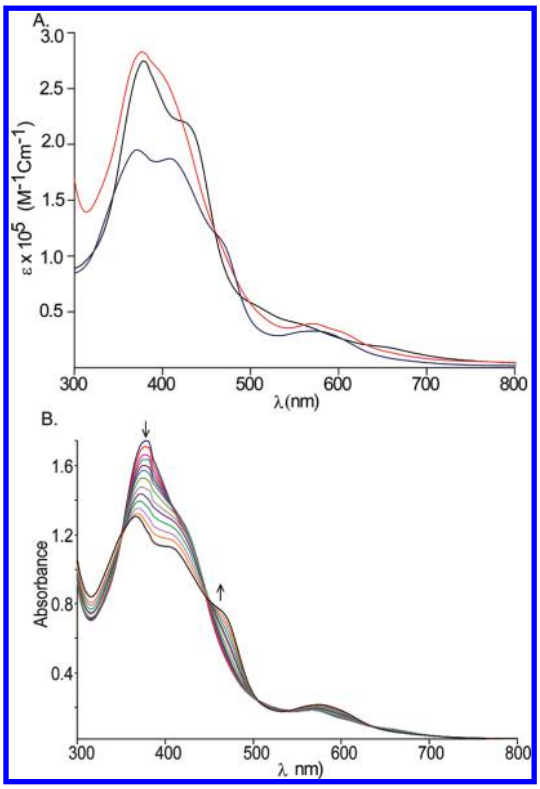

Figure 1. (a) Electronic spectra in $CHCl_3$ of Fe^{III}(*tn*-OEP)ClO_4 (red line), Fe^{III}(*tn*-OEP)(1-MeIm)$_2\cdot ClO_4$ (black line), and Fe^{II}(*tn*-OEP)-(1-MeIm)$_2$ (blue line). (b) Time-evolution spectral changes (at 298 K) of Fe^{III}(*tn*-OEP)ClO_4 in chloroform in the presence of an excess of 1-MeIm in air showing first the appearance of six-coordinated Fe^{III}(*tn*-OEP)-(1-MeIm)$_2\cdot ClO_4$, which upon longer exposure converts to Fe^{II}(*tn*-OEP)-(1-MeIm)$_2$. Arrows indicate an increase or decrease of the band intensity.

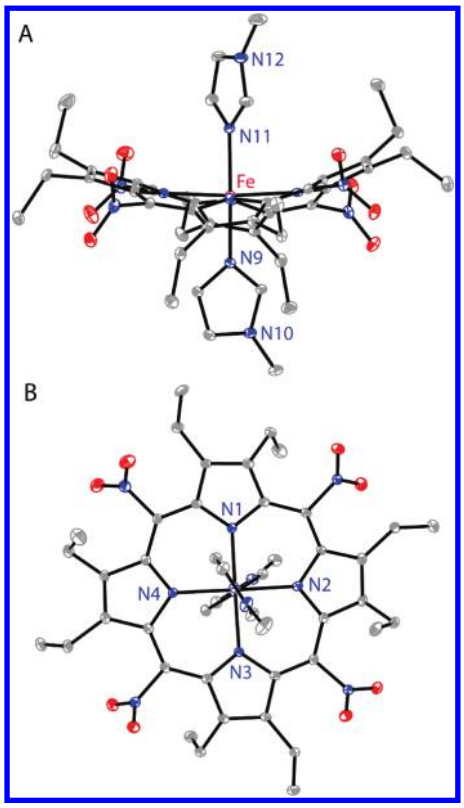

Figure 2. Two perspective views [A, side view; B, top view] of Fe^{II}(*tn*-OEP)(1-MeIm)$_2$ showing 50% thermal contours for all non-hydrogen atoms at 100 K (hydrogen atoms have been omitted for clarity).

piperidine, cyanide, *n*-hexanethiol, phosphine, alkoxides, etc. Two types of mechanisms are known for autoreduction. One is base-catalyzed autoreduction using piperidine, alkoxide, cyanides, etc., which demonstrates that iron reduction is accompanied by one-electron oxidation of the substrates.[33d−g] The electron-transfer step is facilitated by deprotonation of the coordinated base by the free base. In another mechanism, the iron atom ligated to an electron-deficient macrocycle has strong Lewis acidity, which results in autoreduction to iron(II) porphyrin in the presence of an axial ligand such as pyridine.[33a,b] For example, a dioxoporphodimethene ferric complex, in the presence of pyridine, autoreduces spontaneously to a diamagnetic bis(pyridine)iron(II) complex while the corresponding iron(III) octaethylporphyrin derivatives do not.[33b] The ease of reduction is likely a result of the increased Lewis acidity of the iron center. However, to the best of our knowledge, there has been no case in which the imidazoles induce the autoreduction of the iron(III) porphyrin. The observation, as seen here, is very indicative of the fact that the iron atom in Fe^{III}(*tn*-OEP)$(L)_2\cdot X$ has strong Lewis acidity and the four tetranitro substituents at the meso positions shift the redox potential of the iron to significantly positive (vide infra).

Crystallographic Characterization of Fe^{II}(*tn*-OEP)-(1-MeIm)$_2$. Dark-green crystals of the molecule are grown by the slow diffusion of methanol into a chloroform solution of Fe^{III}(*tn*-OEP)ClO_4 containing 5% 1-MeIm at room temperature in air. The complex crystallizes in the triclinic crystal system with a $P\bar{1}$ space group in which one full molecule is present in the asymmetric unit. A perspective view of the molecule is shown in Figure 2, and the selected bond distances and angles are given in Table 1. Fe−Np distances are in the narrow range of 1.977−1.987 Å, while Fe−N_{ax} distances are 2.000(2) and 2.007(2) Å. These distances fall within the spread of literature values[34] observed for low-spin iron(II) porphyrinates containing two planar axial ligands. The planar axial ligands (1-MeIm) make a 80.9° angle with each other and also form 32.2 and 23.8° dihedral angles between the plane of the closest N_p−Fe−N_{ax} and the axial ligand plane.

Another isostructural form of the molecule is obtained by the slow diffusion of cyclohexane into the tetrahydrofuran (THF) solution of Fe^{III}(*tn*-OEP)ClO_4 containing 5% 1-MeIm and also crystallized in the same $P\bar{1}$ space group. The selected bond distances and angles are also given in Table 1, while crystal data and data collection parameters for all of the complexes are reported in Table 2. In the asymmetric unit, one full molecule of the complex along with a THF solvent is present. The Fe−Np distances are also similar and in the narrow range of 1.981(3)−1.990(3) Å, while Fe−N(L) distances are 1.999(3) and 2.002(3) Å. In the molecule, two planar

(34) (a) Li, J.; Nair, S. M.; Noll, B. C.; Schulz, C. E.; Scheidt, W. R. *Inorg. Chem.* **2008**, *47*, 3841. (b) Silvernail, N. J.; Noll, B. C.; Scheidt, W. R. *Acta Crystallogr., Sect. E* **2005**, *E61*, m1201. (c) Hu, C.; Noll, B. C.; Schulz, C. E.; Scheidt, W. R. *Inorg. Chem.* **2005**, *44*, 4346. (d) Safo, M. K.; Scheidt, W. R.; Gupta, G. P. *Inorg. Chem.* **1990**, *29*, 626. (e) Steffen, W. L.; Chun, H. K.; Hoard, J. L.; Reed, C. A. *Abstracts of Papers*; 175th National Meeting of the American Chemical Society, Anaheim, CA, March 13, 1978; American Chemical Society: Washington, DC, 1978; INOR 15.

Table 1. Selected Bond Distances (Å) and Angles (deg)

	Fe^{II}(*tn*-OEP)(1-MeIm)$_2$	Fe^{II}(*tn*-OEP)(1-MeIm)$_2$·THF
	Bond Length (Å)	
Fe−N1	1.977(2)	1.984(3)
Fe−N2	1.978(2)	1.990(3)
Fe−N3	1.987(2)	1.981(3)
Fe−N4	1.987(2)	1.985(3)
Fe−N9	2.000(2)	2.002(3)
Fe−N11	2.007(2)	1.999(3)
	Bond Angle (deg)	
N1−Fe−N2	90.34(9)	89.69(10)
N1−Fe−N3	174.53(9)	173.89(11)
N1−Fe−N4	90.39(9)	89.92(10)
N2−Fe−N3	90.46(9)	89.84(10)
N2−Fe−N4	174.11(9)	175.09(10)
N3−Fe−N4	89.36(9)	91.06(10)
N1−Fe−N9	92.79(9)	93.15(11)
N2−Fe−N9	87.52(9)	87.93(10)
N3−Fe−N9	92.64(9)	92.92(11)
N4−Fe−N9	86.61(9)	87.20(10)
N1−Fe−N11	87.14(9)	87.34(10)
N2−Fe−N11	92.88(9)	92.96(10)
N3−Fe−N11	87.42(9)	86.60(10)
N4−Fe−N11	92.99(9)	91.91(10)
N9−Fe−N11	179.60(9)	178.98(11)

Table 2. Crystal Data and Data Collection Parameters

	Fe^{II}(*tn*-OEP)(1-MeIm)$_2$	Fe^{II}(*tn*-OEP)-(1-MeIm)$_2$·THF
T, K	100(2)	100(2)
formula	C_{44} H_{52} Fe N_{12} O_8	C_{48} H_{60} Fe N_{12} O_9
fw	932.83	1004.93
color and habit	dark green	dark green
cryst syst	triclinic	triclinic
space group	$P\bar{1}$	$P\bar{1}$
a, Å	13.2034(13)	13.2647(8)
b, Å	13.8242(13)	13.3189(8)
c, Å	14.5952(15)	15.7911(9)
α, deg	67.236(2)	68.0510(10)
β, deg	63.902(2)	67.6490(10)
γ, deg	87.045(2)	76.9410(10)
V, Å^3	2183.3(4)	2381.8(2)
radiation (*λ*, Å)	Mo Kα (0.710 73)	Mo Kα (0.710 73)
Z	2	2
d_{calcd}, g cm^{-3}	1.419	1.401
μ, mm^{-1}	0.414	0.387
F(000)	980	1060
no. of unique data	8398	8464
no. of restraints	0	12
no. of params. refined	616	662
GOF on F^2	1.036	1.020
R1[a] [$I > 2\sigma(I)$]	0.0534	0.0577
R1[a] (all data)	0.0694	0.0821
wR2[b] (all data)	0.1438	0.1600

[a] $R1 = \sum||F_o| - |F_c||/\sum|F_o|$. [b] $wR2 = \{\sum[w(F_o^2 - F_c^2)^2]/\sum[w(F_o^2)^2]\}^{1/2}$.

1-MeIm axial ligands are almost perpendicular in orientation in space and make 89.8° angles with each other with 30.0 and 30.3° dihedral angles from the nearest N_p−Fe−N_{ax} plane. The structures of the molecule in two different crystalline forms are quite similar in all important aspects (Table 1); however, they differ in the dihedral angles between the two axial ligands (80.9 and 89.8° for Fe^{II}(*tn*-OEP)(1-MeIm)$_2$ and Fe^{II}(*tn*-OEP)-(1-MeIm)$_2$·THF, respectively). Figures 3 and 4 show the packing diagrams of both molecules. As seen in the diagram, one of the imidazoles is aligned parallel with

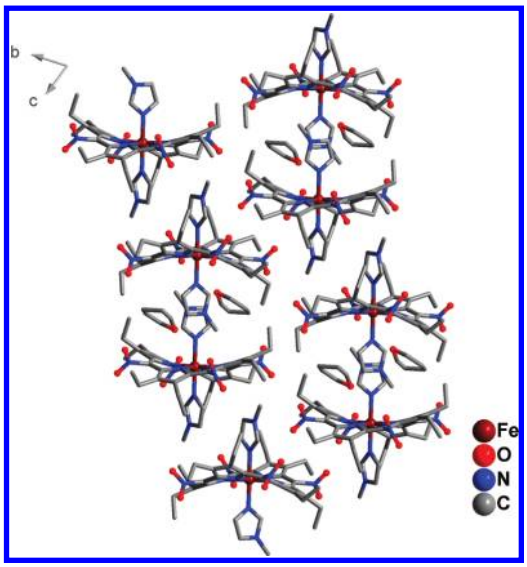

Figure 3. Diagram illustrating the packing of the Fe^{II}(*tn*-OEP)-(1-MeIm)$_2$·THF molecules.

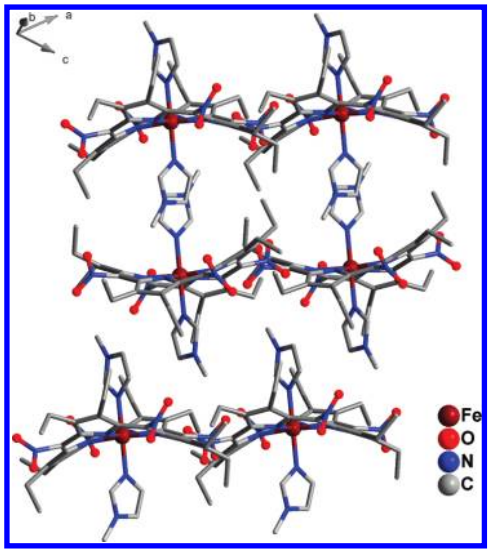

Figure 4. Diagram illustrating the packing of the Fe^{II}(*tn*-OEP)-(1-MeIm)$_2$ molecules.

3.35 and 3.37 Å separations, respectively (the centroid-to-centroid distances are 4.03 and 4.21 Å, respectively) for Fe^{II}(*tn*-OEP)(1-MeIm)$_2$ and Fe^{II}(*tn*-OEP)(1-MeIm)$_2$·THF, which suggest relatively stronger $\pi-\pi$ interactions between the axial imidazoles for the former. The difference of 8.9° in the dihedral angle may be attributable to the relatively stronger $\pi-\pi$ interaction between the axial 1-MeIm in the crystal packing of Fe^{II}(*tn*-OEP)-(1-MeIm)$_2$, which, however, restricts the axial ligand movements to some extent.

Table 3 compares all of the key structural parameters for Fe^{II}(por)L_2 reported here and elsewhere[34] that contain imidazoles as axial ligand L. As can be seen, complexes such as Fe(TPP)(1-VinIm)$_2$, Fe(TPP)(1-BzylIm)$_2$, and Fe-(TPP)(1-MeIm)$_2$, have nearly planar porphyrin cores as well as uncrowded imidazoles as axial ligands and stabilize the parallel orientation of axial ligands.[34d] Bis(imidazole)-ligated iron(II) "picket fence" porphyrinates such as Fe-(TpivPP)(1-MeIm)$_2$, Fe(TpivPP)(1-EtIm)$_2$, and Fe(TpivPP)-

Table 3. Selected Structural Parameters for $Fe^{II}(Porph)(L)_2$ (Where L = Imidazoles)

compound	Fe−N_p [a]	Fe−N_{ax}	Φ [b]	θ [c]	Δ_{24} [d]	C_m [e]	C_β [f]	ref
Fe^{II}(*tn*-OEP)(1-MeIm)$_2$	1.982(2)	2.000(2), 2.007(2)	32.2, 23.8	80.9	0.46	0.22	0.89	Tw
Fe^{II}(*tn*-OEP)(1-MeIm)$_2$·THF	1.985(3)	1.999(3), 2.002(3)	30.0, 30.3	89.8	0.44	0.21	0.83	Tw
Fe(TMP)(2-MeIm)$_2$ mol-1	1.964(5)	2.030(3), 2.047(3)	41.1, 41.4	82.4	0.25	0.51	0.20	34c
Fe(TMP)(2-MeIm)$_2$ mol-2	1.961(7)	2.032(3), 2.028(3)	44.8, 37.9	84.4	0.25	0.50	0.20	34c
Fe(TPP)(4-MeIm)$_2$	1.9952(8)	2.0154(8)	0.7	0		nearly planar		34b
Fe(TPP)(1-VinIm)$_2$	2.001(2)	2.004(2)	14	0		nearly planar		34d
Fe(TPP)(1-BzylIm)$_2$	1.993(9)	2.017(4)	26	0		nearly planar		34d
Fe(TPP)(1-MeIm)$_2$	1.997(6)	2.014(5)	15	0		nearly planar		34e
Fe(TpivPP)(1-MeIm)$_2$	1.992(3)	1.9958(19), 1.9921(18)	8.5, 21.1	77.2		nearly planar		34a
Fe(TpivPP)(1-EtIm)$_2$	1.993(6)	2.0244(18), 1.9940(19)	6.6, 20.7	62.4		nearly planar		34a
Fe(TpivPP)(1-VinylIm)$_2$	1.988(5)	1.9979(19), 1.9866(18)	11.2, 24.5	78.5		nearly planar		34a

[a] Average value in angstroms. [b] Dihedral angle between the plane of the closest Np−Fe−N_{ax} and the axial ligand plane. [c] Dihedral angle between two axial ligands. [d] Average displacement of the 24 atoms from the least-squares plane of the porphyrin. [e] Average displacement of *meso*-carbon atoms from the least-squares plane of the porphyrin (24 atoms). [f] Average displacement of *beta*-carbon atoms from the least-squares plane of the porphyrin (24 atoms).

(1-VinylIm)$_2$ have nearly perpendicular axial orientation, although they all have nearly planar porphyrin cores and unhindered imidazoles as axial ligands. In these cases, the "picket fence" environment provides strong steric interactions, forcing the axial ligands to arrange in perpendicular orientations.[34a] For Fe(TMP)(2-MeIm)$_2$, however, a near-perpendicular ligand orientation is due to coordination of bulky 2-MeIm as axial ligands, which also results from a strongly ruffled porphyrin core. In sharp contrast to all earlier reports, our molecules Fe^{II}(*tn*-OEP)(L)$_2$ demonstrate near-perpendicular axial ligand orientation even with unhindered imidazoles as axial ligands in a distorted macrocyclic environment.

The porphyrin rings are highly distorted in the complexes reported here and are best appreciated by turning to Figure 5, where the out-of-plane displacements in units of 0.01 Å of the porphyrin core atoms are compared along with reported[9a−d] iron complexes with the same macrocycle. The nomenclature that describes the types of distortions commonly observed in nonplanar porphyrins was originally suggested by Scheidt and Lee.[35] In a saddle conformation, alternating pyrrole rings tilt up and down with respect to the porphyrin mean plane (24 atoms) and the *meso*-carbon atoms lie on the least-squares plane. In a ruffled conformation, alternating pyrrole rings twist clockwise or counterclockwise about the metal nitrogen bond and the *meso*-carbon atoms move alternately above or below the least-squares plane of the 24 porphyrin atom core. As is evident from Figure 5, the ring distortions of all of the complexes can be described as the saddle type with alternating displacement of the pyrrole rings below and above the mean porphyrin plane.

Table 4 describes selected structural parameters for all of the iron complexes containing *tn*-OEP as the porphyrin core. Although complexes are mostly saddle-distorted, the cores in Fe^{III}(*tn*-OEP)$(H_2O)_2$·ClO_4 and the ferrous porphyrin Fe^{II}(*tn*-OEP)(1-MeIm)$_2$ reported here have significant ruffle contributions, which accommodates the steric congestion of the peripheral substituents and helps the metal to be more in-plane, as observed in the series. Shelnutt et al. have developed a normal-coordinate structural decomposition (NSD) method,[36] which simulates any porphyrin distortion by linear combinations of

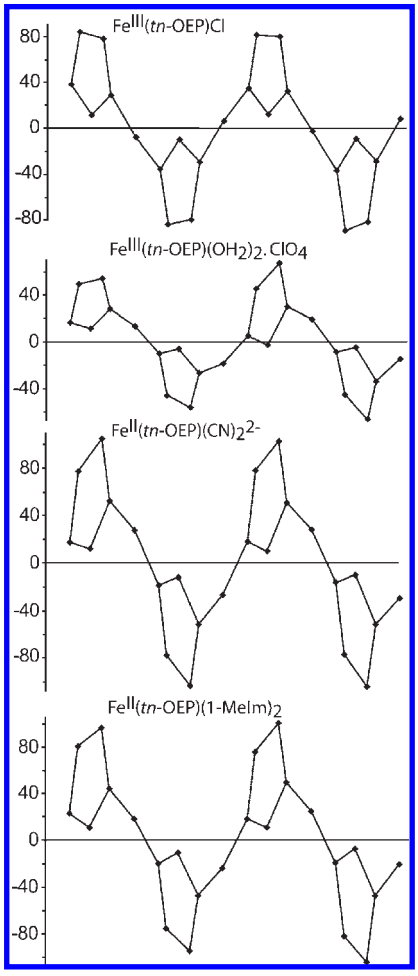

Figure 5. Out-of-plane displacements (in units of 0.01 Å) of the porphyrin core atoms from the mean porphyrin plane.

six normal deformations—saddled (sad), ruffled (ruf), domed (dom), wav(*x*), wav(*y*), and propeller (pro)—and also yield total out-of-plane displacements (D_{oop}). The results of NSD analysis of the complexes are presented in Table 5. The total distortions (D_{oop}) decrease in the order [K(18-crown-6)$(OH_2)_2]_2$[Fe^{II}(*tn*-OEP)$(CN)_2$] > Fe^{II}(*tn*-OEP)(1-MeIm)$_2$ > Fe^{III}(*tn*-OEP)Cl > Fe^{III}(*tn*-OEP)-(MeOH)Cl > Fe^{III}(*tn*-OEP)$(H_2O)_2$·ClO_4. As can be seen from Table 5 and Figure 5, the ferrous porphyrins are more distorted than the corresponding ferric complex.

(35) Scheidt, W. R.; Lee, Y. J. *Struct. Bonding* (*Berlin*) **1987**, *64*, 1.
(36) (a) Jentzen, W.; Ma, J.-G.; Shelnutt, J. A. *Biophys. J.* **1998**, *74*, 753. (b) Jentzen, W.; Song, X.-Z.; Shelnutt, J. A. *J. Phys. Chem. B* **1997**, *101*, 1684.

Table 4. Selected Structural Parameters for the Fe(*tn*-OEP) Core

complex	Fe−N_p[a]	Fe−L_{ax}[a]	$\Delta^{Fe}{}_{4N}$[b]	Δ_{24}[c]	C_m[d]	C_β[e]	core size	ref
Fe^{III}(*tn*-OEP)Cl	2.067(3)	2.1918(10)	0.46	0.41	0.06	0.82	2.014	9a
Fe^{III}(*tn*-OEP)(MeOH)Cl	2.064(3)	2.170(3), 2.3049(11)	0.13	0.36	0.05	0.76	2.060	9a
Fe^{III}(*tn*-OEP)$(H_2O)_2\cdot ClO_4$	2.061(2)	2.070(4)	0.00	0.28	0.17	0.54	2.061	9a
K(18-crown-6)$(OH_2)_2]_2[Fe^{II}$(*tn*-OEP)$(CN)_2]$	1.982(3)	1.988(4)	0.00	0.48	0.28	0.91	1.982	9c
Fe^{II}(*tn*-OEP)$(1\text{-MeIm})_2$	1.982(2)	2.003(2)	0.00	0.46	0.22	0.89	1.982	Tw
Fe^{II}(*tn*-OEP)$(1\text{-MeIm})_2\cdot$THF	1.985(3)	2.000(3)	0.01	0.44	0.21	0.83	1.985	Tw

[a] Average value in anstroms. [b] Displacement of iron from the mean plane containing four porphyrinic nitrogen atoms. [c] Average displacement of the 24 atoms from the least-squares plane of the porphyrin. [d] Average displacement of *meso*-carbon atoms from the least-squares plane of the porphyrin (24 atoms). [e] Average displacement of *beta*-carbon atoms from the least-squares plane of the porphyrin (24 atoms).

Table 5. NSD[35,36] of the Fe(*tn*-OEP) Complexes

complex	D_{oop}	B2u, saddle	B1u, ruffle	A2u, dome	Eg(*x*), wave(*x*)	Eg(*y*), wave(*y*)	A1u, propeller	sum	ruf/sum (%)
Fe^{III}(*tn*-OEP)Cl	2.5186	−2.5118	−0.1676	−0.0443	−0.0018	0.0622	−0.0175	2.8052	5.97
Fe^{III}(*tn*-OEP)(MeOH)Cl	2.3026	−2.2888	0.0750	0.1317	0.0186	−0.2000	−0.0091	2.7232	2.75
Fe^{III}(*tn*-OEP)$(H_2O)_2.ClO_4$	1.6926	1.6193	−0.4797	−0.0131	0.0343	0.1015	−0.0270	2.2749	21
Fe^{II}(*tn*-OEP)$(1\text{-MeIm})_2$	2.7581	−2.6789	−0.6461	−0.0191	0.0147	0.1134	−0.0069	3.4791	18.5
Fe^{II}(*tn*-OEP)$(1\text{-MeIm})_2$.THF	2.6072	−2.5189	−0.6389	0.0929	0.0144	−0.1882	0.0045	3.4578	18.47
[K(18-crown-6)$(OH_2)_2]_2[Fe^{II}$(*tn*-OEP)$(CN)_2]$	2.8597	−2.7389	−0.8223	0.0011	0.0153	−0.0076	0.0009	3.5861	22.9

However, the saddling contribution decreases sharply from ferric to ferrous, while the ruffling contribution increases significantly in the series. The porphyrin core is least distorted in Fe^{III}(*tn*-OEP)$(H_2O)_2\cdot ClO_4$, which also has the highest core size (2.061 Å), while the highly distorted vis-à-vis core size (1.982 Å) is lowest in Fe^{II}(*tn*-OEP)$(1\text{-MeIm})_2$, which shows a significant core expansion of 0.08 Å in the series. The large size of the high-spin iron(III) atom in Fe^{III}(*tn*-OEP)$(H_2O)_2\cdot ClO_4$ is accommodated by a substantial radial expansion of the porphyrin core with no displacement of the metal, while the lower size of low-spin iron(II) can be fitted well by the substantial contraction of the same ring or vice versa. Thus, our characterization demonstrates that an increase in ruffling and/or a decrease in macrocycle deformation causes the iron atom to be more in-plane in a distorted macrocyclic environment. Our demonstration also suggests that varieties of oxidation and spin states of iron porphyrins, which are critical intermediates in the catalytic cycles of biological systems, are consequences of axial coordination as well as the nature and extent of protein-induced deformations at the heme and can account, at least in part, for the various functions of chemically similar tetrapyrrole pigments found in nature.

DFT calculations have been carried out for Fe^{II}(*tn*-OEP)$(1\text{-MeIm})_2$, in which the atom coordinates are taken from the single-crystal X-ray data of the molecule. Full geometry optimization has been obtained using DFT, specifically the Becke three-parameter exchange functional (B3)[38] and the Lee−Yang−Parr correlation functional (LYP).[39] These B3LYP calculations have been carried out with the *Gaussian 03*, revision B.04, package.[40] On the basis of geometry optimization, the energy minimum occurs at the geometry where the two 1-MeIm are oriented nearly perpendicular with a 82.54° dihedral angle, which is also in close agreement with the 80.9° angle observed in the X-ray structure of Fe^{II}(*tn*-OEP)$(1\text{-MeIm})_2$. The selected bond distances and angles are shown in Table S1 (see the Supporting Information), where they are compared with the values obtained from X-ray structures of the molecule. Even starting from parallel axial orientations of 1-MeIm, the geometry optimization converged to the perpendicular axial alignment. The NSD analysis shows that the porphyrin core is exclusively saddle-distorted (92.4%) in the optimized structure while the X-ray structure of the molecule shows 77% saddle with a significant ruffle contribution of 18.5%. Our observation thus demonstrates conclusively that the relatively perpendicular axial orientations are preferred for unhindered and planar

(37) (a) Hu, C.; Noll, B. C.; Schulz, C. E.; Scheidt, W. R. *Inorg. Chem.* **2006**, *45*, 9721. (b) Yatsunyk, L. A.; Carducci, M. D.; Walker, F. A. *J. Am. Chem. Soc.* **2003**, *125*, 15986. (c) Ogura, H.; Yatsunyk, L.; Medforth, C. J.; Smith, K. M.; Barkigia, K. M.; Renner, M. W.; Melamed, D.; Walker, F. A. *J. Am. Chem. Soc.* **2001**, *123*, 6564. (d) Silver, J.; Marsh, P. J.; Symons, M. C.; Svistunenko, D. A.; Frampton, C. S.; Fern, G. R. *Inorg. Chem.* **2000**, *39*, 2874. (e) Munro, O. Q.; Serth-Guzzo, J. A.; Turowska-Tyrk, I.; Mohanrao, K.; Shokhireva, T. Kh.; Walker, F. A.; Debrunner, P. G.; Scheidt, W. R. *J. Am. Chem. Soc.* **1999**, *121*, 11144. (f) Munro, O. Q.; Marques, H. M.; Debrunner, P. G.; Mohanrao, K.; Scheidt, W. R. *J. Am. Chem. Soc.* **1995**, *117*, 935. (g) Safo, M. K.; Gupta, G. P.; Walker, F. A.; Scheidt, W. R. *J. Am. Chem. Soc.* **1991**, *113*, 5497. (h) Higgins, T.; Safo, M. K.; Scheidt, W. R. *Inorg. Chim. Acta* **1990**, *178*, 261. (i) Scheidt, W. R.; Osvath, S. R.; Lee, Y. J. *J. Am. Chem. Soc.* **1987**, *109*, 1958. (j) Scheidt, W. R.; Kirner, J. F.; Hoard, J. L.; Reed, C. A. *J. Am. Chem. Soc.* **1987**, *109*, 1963. (k) Geiger, D. K.; Lee, Y. J.; Scheidt, W. R. *J. Am. Chem. Soc.* **1984**, *106*, 6339. (l) Little, R. G.; Dymock, K. R.; Ibers, J. A. *J. Am. Chem. Soc.* **1975**, *97*, 4532. (m) Collins, D. M.; Countryman, R.; Hoard, J. L. *J. Am. Chem. Soc.* **1972**, *94*, 2066.

(38) Becke, A. D. *J. Chem. Phys.* **1993**, *98*, 5648.

(39) Lee, C.; Yang, W.; Parr, R. G. *Phys. Rev. B.* **1988**, *37*, 785.

(40) Frisch, M. J.; Trucks, G. W.; Schlegel, H. B.; Scuseria, G. E.; Robb, M. A.; Cheeseman, J. R.; Montgomery, J. A., Jr.; Vreven, T.; Kudin, K. N.; Burant, J. C.; Millam, J. M.; Iyengar, S. S.; Tomasi, J.; Barone, V.; Mennucci, B.; Cossi, M.; Scalmani, G.; Rega, N.; Petersson, G. A.; Nakatsuji, H.; Hada, M.; Ehara, M.; Toyota, K.; Fukuda, R.; Hasegawa, J.; Ishida, M.; Nakajima, T.; Honda, Y.; Kitao, O.; Nakai, H.; Klene, M.; Li, X.; Knox, J. E.; Hratchian, H. P.; Cross, J. B.; Bakken, V.; Adamo, C.; Jaramillo, J.; Gomperts, R.; Stratmann, R. E.; Yazyev, O.; Austin, A. J.; Cammi, R.; Pomelli, C.; Ochterski, J. W.; Ayala, P. Y.; Morokuma, K.; Voth, G. A.; Salvador, P.; Dannenberg, J. J.; Zakrzewski, V. G.; Dapprich, S.; Daniels, A. D.; Strain, M. C.; Farkas, O.; Malick, D. K.; Rabuck, A. D.; Raghavachari, K.; Foresman, J. B.; Ortiz, J. V.; Cui, Q.; Baboul, A. G.; Clifford, S.; Cioslowski, J.; Stefanov, B. B.; Liu, G.; Liashenko, A.; Piskorz, P.; Komaromi, I.; Martin, R. L.; Fox, D. J.; Keith, T.; Al-Laham, M. A.; Peng, C. Y.; Nanayakkara, A.; Challacombe, M.; Gill, P. M. W.; Johnson, B.; Chen, W.; Wong, M. W.; Gonzalez, C.; Pople, J. A. *Gaussian 03*, revision B.04; Gaussian, Inc.: Pittsburgh, PA, **2003**.

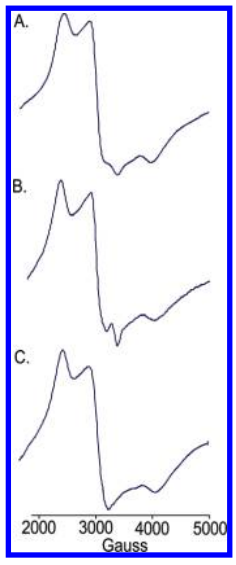

Figure 6. X-band EPR spectrum in toluene (at 77 K) of (A) Fe^{III}(*tn*-OEP)(4-MeIm)$_2\cdot ClO_4$, (B) Fe^{III}(*tn*-OEP)(1-MeIm)$_2\cdot ClO_4$, and (C) Fe^{III}-(*tn*-OEP)(1-MeIm)$_2\cdot$Cl.

imidazoles as axial ligands in the highly saddled-distorted iron(II) tetranitrooctaethylporphyrin.

We are unable to get X-ray-quality crystals of Fe^{III}-(*tn*-OEP)(L)$_2\cdot ClO_4$ suitable for structure determinations. However, EPR spectra of the molecules in both the solid and solution phases at 77 K are measured, and two of them are also shown in Figure 6. The spectra (solid state, 77 K) are of the rhombic type with $g_3 = 2.79$, $g_2 = 2.32$, and $g_1 = 1.69$ ($\sum g^2 = 16.02$) for Fe^{III}(*tn*-OEP)(1-MeIm)$_2\cdot ClO_4$; $g_3 = 2.84$, $g_2 = 2.27$, and $g_1 = 1.67$ ($\sum g^2 = 16.01$) for Fe^{III}-(*tn*-OEP)(Im)$_2\cdot ClO_4$; and $g_3 = 2.83$, $g_2 = 2.28$, and $g_1 = 1.68$ ($\sum g^2 = 16.03$) for Fe^{III}(*tn*-OEP)(4-MeIm)$_2\cdot ClO_4$. Similar rhombic spectra are also observed in the solution phase (see the Experimental Section for details). To explore further the effect of counteranion, we have also synthesized and characterized[41] Fe^{III}(*tn*-OEP)(L)$_2\cdot$Cl by adding L on Fe^{III}(*tn*-OEP)Cl using a procedure identical with that used for Fe^{III}(*tn*-OEP)(L)$_2\cdot ClO_4$. The rhombic EPR spectra are also observed[41] for Fe^{III}(*tn*-OEP)(L)$_2\cdot$Cl (Figure 6). Such types of spectra are typical for low-spin ($S = {}^1/_2$) iron(III) porphyrins.

One of the most useful spectroscopic tools that provides much insight into the relative axial orientation and electronic configuration of the low-spin iron(III) center is EPR spectroscopy. The EPR spectra of low-spin, six-coordinated iron(III) hemes have been divided into three types.[4] Type I complexes exhibit "large g_{max}" EPR spectra, where one prominent resonance at $g > 3.2$ dominates the spectrum. Such complexes have a $(d_{xy})^2(d_{xz}, d_{yz})^3$ electronic configuration. If planar axial ligands are present, these ligands are arranged so that their planes are nearly perpendicular. Type II porphyrin complexes have rhombic EPR spectra. These also have a $(d_{xy})^2(d_{xz}, d_{yz})^3$ electronic configuration, but with planar axial ligands, the ligand planes are nearly parallel. Finally, type III hemes have axial EPR spectra with $g_\perp \sim 2.6$. Complexes of this type have the less common $(d_{xz}, d_{yz})^4(d_{xy})^1$ electronic ground state. However, our molecule Fe^{III}(*tn*-OEP)-(L)$_2\cdot$X (X = Cl, ClO_4) gives rhombic EPR spectra in both the solid and solution phases at 77 K, which fall under type II with $(d_{xy})^2(d_{xz}, d_{yz})^3$ electronic configuration and thus would stabilize nearly parallel axial ligand orientations. Similar rhombic EPR spectra were also observed before for Fe(OMTPP)(1-MeIm)$_2\cdot$Cl, which have a saddle-distorted porphyrin core with unhindered 1-MeIm as axial ligands; the X-ray structure of the molecule also shows a nearly parallel axial ligand orientation (dihedral angle of 19.5°).[37b] Walker et al. have also shown that a normal rhombic signal can be observed when the dihedral angle between planar axial ligands is as large as 30°.[37b]

Single-point energy calculation was also performed using DFT for Fe^{III}(*tn*-OEP)(1-MeIm)$_2^+$, in which two axial 1-MeIm ligands are kept in both parallel and perpendicular orientations. Coordinates of the molecule are generated from the X-ray structure of the corresponding low-spin iron(II) complex Fe^{II}(*tn*-OEP)(1-MeIm)$_2$, and for the parallel orientation, 1-MeIm ligands are rotated manually. The calculation shows that the energy of the complex with parallel orientations of 1-MeIm is 174.7 kcal mol^{-1} less compared to that of the molecule with perpendicular orientations. It is to be noted here that the complexity of the electronic structure of the molecule and the size of the system are such that we are unable to perform the full geometry optimization. Because the energy difference between the parallel and perpendicular orientations is so large, we expect qualitatively the same result even after the full geometry optimization and experimental results (vide supra) are also in full agreement. Our observation thus demonstrates conclusively that the relatively parallel axial orientations are preferred for planar and unhindered imidazoles in saddled-distorted iron(III) tetranitrooctaethylporphyrin. Previous DFT calculations on Fe^{II}(por)(Im)$_2$ and Fe^{III}-(por)(Im)$_2^+$ (por = porphyrin; Im = imidazole), which have planar porphyrin macrocycles, showed no difference in the preference for parallel or orthogonal orientations of imidazoles because they almost have the same energy.[23,24] This is also in agreement with the experimental data;[25−29] for model hemes with unhindered porphyrins, which do not possess bulky substituents, practically no barrier of rotation was found for axial imidazole ligands.

The orientations of planar axial ligands in bis-(imidazole)-ligated iron(III) porphyrins have been intensively investigated.[37] Table 6 shows all structurally characterized six-coordinated low-spin iron(III) porphyrins containing imidazoles as axial ligands. On the basis of structural and spectroscopic investigations, it was found that, for low-spin d^5 ferriheme centers, parallel orientations of axial imidazole ligands are exclusively observed

(41) Fe^{III}(*tn*-OEP)(L)$_2\cdot$Cl are prepared using the general procedure used for Fe^{III}(*tn*-OEP)(L)$_2\cdot ClO_4$, only Fe^{III}(*tn*-OEP)Cl was used as the starting material instead of Fe^{III}(*tn*-OEP)ClO_4. **Fe^{III}(*tn*-OEP)(1-MeIm)$_2\cdot$Cl**. Yield: 26 mg, 44%. Anal. Calcd (found): C, 54.63 (54.68); H, 5.41 (5.45); N, 17.37 (17.35). UV−vis (benzene) [λ_{max}, nm (ε, M^{-1} cm^{-1})]: 377 (3.46×10^5), 422sh (2.24×10^5), 572 (4.22×10^4). EPR data: in solid (77 K), $g_1 = 1.70$, $g_2 = 2.26$, $g_3 = 2.84$; in toluene (77 K), $g_1 = 1.71$, $g_2 = 2.27$, $g_3 = 2.82$. **Fe^{III}(*tn*-OEP)(4-MeIm)$_2\cdot$Cl**. Yield: 28 mg, 48%. Anal. Calcd (found): C, 54.63 (54.58); H, 5.41 (5.46); N, 17.37 (17.41). UV−vis (benzene) [λ_{max}, nm (ε, M^{-1} cm^{-1})]: 378 (3.18×10^5), 421sh (2.43×10^5), 638 (4.41×10^4). EPR data: in solid (77 K), $g_1 = 1.69$, $g_2 = 2.28$, $g_3 = 2.82$; in toluene (77 K), $g_1 = 1.70$, $g_2 = 2.32$, $g_3 = 2.79$. **Fe^{III}(*tn*-OEP)(Im)$_2\cdot$Cl**. Yield: 26 mg, 45%. Anal. Calcd (found): C, 53.70 (53.74); H, 5.15 (5.18); N, 17.89 (17.85). UV−vis (benzene) [λ_{max}, nm (ε, M^{-1} cm^{-1})]: 376 (3.78×10^5), 423sh (2.96×10^5), 636 (3.67×10^4). EPR data: in solid (77 K), $g_1 = 1.72$, $g_2 = 2.29$, $g_3 = 2.80$; in toluene (77 K), $g_1 = 1.72$, $g_2 = 2.26$, $g_3 = 2.82$.

Table 6. Selected Structural Parameters for $Fe^{III}(Porph)(L)_2^+$ (Where L = Imidazoles)

compound	Fe−N_p[a]	Fe−N_{ax}[a]	θ[b]	C_m[c]	C_β[d]	ref
Fe(TPP)$(Im)_2\cdot Cl\cdot$MeOH	1.989(8)	1.974(24)	57	0.31	0.12	37m
Fe(TPP)$(2\text{-MeIm})_2\cdot ClO_4$	1.971(4)	2.012(4)	89.3	0.40	0.17	37j
Fe(TPP)$(Im)_2\cdot Cl\cdot CHCl_3$	1.994(12), 1.993(4)	1.964(3), 1.977(3)	0	nearly planar		37i
Fe(TPP)$(4\text{-MeIm})_2\cdot Cl$	2.000(11), 1.995(10)	1.975(2), 1.987(2)	0	nearly planar		37d
Fe(TPP)$(1\text{-MeIm})_2\cdot ClO_4$	1.982(11)	1.974(6)	11	nearly planar		37h
Fe(TMP)$(5\text{-MeIm})_2\cdot ClO_4$	1.981(7)	1.965(6)	76	0.32	0.13	37e
Fe(TMP)$(1,2\text{-Me}_2\text{Im})_2\cdot ClO_4$	1.937(12)	2.004	89.4	0.72	0.27	37f
Fe(TMP)$(1\text{-MeIm})_2\cdot ClO_4$	1.988(2), 1.987(1)	1.975(3), 1.965(3)	0	nearly planar		37g
Fe(TMP)$(5\text{-MeIm})_2\cdot ClO_4$	1.983(4), 1.981(5)	1.970(12), 1.982(3)	30, 26	0.11, 0.05	0.16, 0.07	37e
Fe(OMTPP)$(1\text{-MeIm})_2\cdot Cl$	1.969(7)	1.982(10)	90	0.10	0.97	37b
Fe(OMTPP)$(2\text{-MeIm})_2\cdot Cl$	1.977(4)	2.006(5), 2.032(5)	82.1	0.21	0.95	37b
Fe(OMTPP)$(2\text{-MeIm})_2\cdot Cl$	1.979(7)	2.007(7), 2.010(7)	80.7	0.13	1.02	37b
Fe(OMTPP)$(1\text{-MeIm})_2\cdot Cl$	1.990(2)	1.996(29)	19.5	0.01	1.01	37b
Fe(OETPP)$(1\text{-MeIm})_2\cdot Cl$	1.970(7)	1.977(1)	73	0.03	1.23	37b
Fe(OETPP)$(2\text{-MeIm})_2\cdot(SbF_6, Cl)$	1.974(9)	2.09(2)	90	0.09	1.21	37c
Fe(TC_6TPP)$(1\text{-MeIm})_2\cdot Cl$	2.005(3)	2.005(8)	90.0	0.26	0.5	37b
Fe(OEP)$(2\text{-MeIm})_2\cdot Cl$	1.974(4)	2.005(10)	87.6	0.46	0.18	37a
Fe(OEP)$(2\text{-MeIm})_2\cdot ClO_4$	2.041(9)	2.275(1)	0	nearly planar		37k
Fe(Proto IX)$(1\text{-MeIm})_2$	1.991(16)	1.977(16)	13	nearly planar		37l

[a] Average value in anstroms. [b] Dihedral angle between the two axial ligands. [c] Average displacement of *meso*-carbon atoms from the least-squares plane of the porphyrin (24 atoms). [d] Average displacement of *beta*-carbon atoms from the least-squares plane of the porphyrin (24 atoms).

for planar porphyrins, while highly nonplanar porphyrin geometries are required to force the relative perpendicular orientation of planar axial ligands. Another set of strategies used with success in iron(III) to force relative perpendicular orientations is the use of sterically hindered imidazoles such as 2-methylimidazole (2-MeIm). It is, however, interesting to note the presence of both parallel and perpendicular axial ligand orientations for the $Fe^{III}(OEP)(2\text{-MeIm})_2^+$ core. The elongation of the Fe−N_p and Fe−N_{ax} bond distances in $Fe^{III}(OEP)(2\text{-MeIm})_2\cdot ClO_4$ provides a means for alleviating steric contacts, and the nearly planar porphyrin core also leads to parallel orientations of the axial ligands, which are found to be in the high-spin state in the crystalline phase.[37k] On the other hand, short Fe−N_p and Fe−N_{ax} distances for $Fe^{III}(OEP)(2\text{-MeIm})_2\cdot Cl$ results in a highly nonplanar porphyrin core, which along with hindered 2-MeIm leads to nearly perpendicular axial orientations, and the spin state of the molecule was shown to be low-spin.[37a] In the molecule, the coordinated imidazole ligands form hydrogen bonds with the chloride counteranions and provide a probable explanation for the apparently stronger ligand field observed in $Fe^{III}(OEP)(2\text{-MeIm})_2\cdot Cl$.[37a] Another interesting complex reported was $Fe(OMTPP)(1\text{-MeIm})_2\cdot Cl$, which has been obtained in two crystalline forms with distinctly different axial ligand orientations. One form, *perp*-$Fe(OMTPP)(1\text{-MeIm})_2\cdot Cl$, has axial ligands in strictly perpendicular planes; the second form, *paral*-$Fe(OMTPP)(1\text{-MeIm})_2\cdot Cl$, has a nearly parallel axial ligand orientation with a dihedral angle of 19.5°.[37b]

The complex $Fe^{III}(tn\text{-OEP})(L)_2\cdot X$ (X = Cl, ClO_4) shows the rhombic EPR signals at 77 K in both the solid and solution phases and thus represents very rare examples of nearly parallel axial orientations for the unhindered and planar imidazoles in a saddle-distorted porphyrin macrocycle. The results are also supported by the single-point energy calculation using DFT. We have also seen that, by changing the counteranion from ClO_4^- to Cl^- for $Fe^{III}(tn\text{-OEP})(L)_2^+$, the spin state (low-spin) and the relative ligand orientation remain the same. Walker et al., however, have shown that a normal rhombic signal can be observed when the dihedral angle between the planar axial ligands is as large as 30°.[37b]

Cyclic Voltammetric Study. Cyclic voltammetric experiments for $Fe^{III}(tn\text{-OEP})ClO_4$ are done at 25 °C under dinitrogen in CH_2Cl_2 with 0.1 M tetrabutylammonium perchlorate (TBAP) as the supporting electrolyte; $E_{1/2}$ of the Fe^{III}/Fe^{II} reduction process is observed at 0.22 V (ΔE_p, 75 mV), a considerably more positive value than those of Fe(*tn*-OEP)Cl and Fe(OEP)Cl, which were found[9a] at 0.20 and −0.49 V, respectively, under identical condition. However, the ring-centered oxidation of $Fe^{III}(tn\text{-OEP})ClO_4$ is not observed within the solvent limit (~1.8 V).

The complex $Fe^{II}(tn\text{-OEP})(L)_2$ is also redox-active in solution under identical conditions, and a typical voltammogram for $Fe^{II}(tn\text{-OEP})(1\text{-MeIm})_2$ is shown in Figure 7. $E_{1/2}$ of the Fe^{II}/Fe^{III} oxidation process is observed at a considerably higher positive value of 0.49 V for 1-MeIm. The observed one-electron oxidation of Fe^{II} to Fe^{III} at such high positive potentials for $Fe^{II}(tn\text{-OEP})(L)_2$ readily explains why the complexes are so stable in air. Bulk oxidation of $Fe^{II}(tn\text{-OEP})(1\text{-MeIm})_2$ in dichloromethane at a constant potential of 0.69 V under nitrogen changes the color from green to brown; the oxidized product is identified as $Fe^{III}(tn\text{-OEP})(1\text{-MeIm})_2\cdot ClO_4$ and shows the same EPR spectrum at 77 K. The species again upon reduction at 0.29 V regenerates the green solution of $Fe^{II}(tn\text{-OEP})(1\text{-MeIm})_2$.

Conclusions

We have reported here the addition of axial imidazole ligands on $Fe^{III}(tn\text{-OEP})ClO_4$, which first forms $Fe^{III}(tn\text{-OEP})(L)_2\cdot ClO_4$ and then spontaneously autoreduces in the presence of excess axial ligands to the rare air-stable $Fe^{II}(tn\text{-OEP})(L)_2$. Our molecule $Fe^{III}(tn\text{-OEP})ClO_4$ shows a nearly pure high-spin nature in both the solid and solution phases. In contrast, all reported $Fe^{III}(por)ClO_4$ complexes are either mixed or intermediate spin states. X-ray structures of $Fe^{II}(tn\text{-OEP})(1\text{-MeIm})_2$ and $Fe^{II}(tn\text{-OEP})(1\text{-MeIm})_2\cdot THF$ are reported that demonstrated, for the first time, the near-perpendicular axial ligand orientation (dihedral angles of

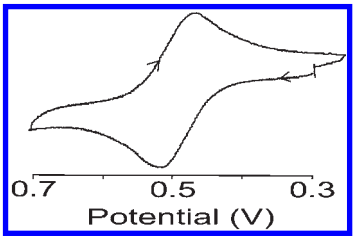

Figure 7. Portion of the cyclic voltammogram for Fe^{II}(*tn*-OEP)-(1-MeIm)$_2$ in CH_2Cl_2 (scan rate of 100 mV s^{-1}) with 0.1 M TBAP as the supporting electrolyte. The reference electrode was Ag/AgCl.

80.9 and 89.8°, respectively) for iron(II) porphyrins in a highly distorted macrocyclic environment. Even starting from parallel axial orientations of 1-MeIm, the geometry optimization using DFT converged to the perpendicular axial alignment with a 82.54° dihedral angle. This is in sharp contrast to all earlier reports where sterically crowded imidazole or a nearly planar porphyrin core with a "picket fence" environment to restrict the rotation of the axial ligands is required for perpendicular orientation. Electrochemical data obtained from a cyclic voltammetric study of Fe^{II}(*tn*-OEP)(L)$_2$ reveal the one-electron oxidation at very high positive potential, which readily explains why the complexes are so stable in air.

On the basis of structural and spectroscopic investigations, it was found earlier that, for low-spin d^5 ferriheme centers, parallel orientations of axial imidazole ligands are exclusively observed for planar porphyrins while highly nonplanar porphyrin geometries are required to force the relative perpendicular orientation of planar axial ligands in iron(III) porphyrinates. Another set of strategies used with success in iron(III) to force perpendicular orientations of axial ligands was the use of sterically hindered imidazoles such as 2-MeIm. However, our molecule Fe^{III}(*tn*-OEP)(L)$_2\cdot$X (X = Cl, ClO_4) gives rhombic EPR spectra in both the solid and solution phases at 77 K and represents rare examples of nearly parallel axial orientations for the planar and unhindered imidazoles using the saddle-distorted porphyrin macrocycle. Single-point energy calculation was also performed on Fe^{III}-(*tn*-OEP)(1-MeIm)$_2^+$ using DFT, which shows that the parallel alignment of 1-MeIm is preferred compared to the perpendicular alignment. Bulk oxidation of Fe^{II}(*tn*-OEP)(1-MeIm)$_2$ in dichloromethane with 0.1 M TBAP as the supporting electrolyte at a constant potential of 0.69 V generates Fe^{III}(*tn*-OEP)(1-MeIm)$_2\cdot ClO_4$, which has the same EPR spectrum, which upon reduction at 0.29 V regenerates Fe^{II}-(*tn*-OEP)(1-MeIm)$_2$ again. Thus, we have demonstrated here, for the first time, that iron(II) and iron(III) porphyrinates with two planar and unhindered axial ligands have different orientation preferences in a nonplanar porphyrinic environment. In both Fe^{II}(*tn*-OEP)(L)$_2$ and Fe^{III}(*tn*-OEP)-(L)$_2\cdot$X, the peripheral substituents are all same and their effects are thus expected to be similar. However, the conformation and electronic effect should be operative, leading to two different axial orientations in both cases, although the exact origin is still unclear at this stage.

Experimental Section

Materials. Reagents and solvents were purchased from commercial sources and purified by standard procedures before previously. Grade I neutral alumina was used for column chromatography. [Fe^{III}(*tn*-OEP)]$_2$O was prepared by literature methods.[9d]

Preparation of Fe^{III}(*tn*-OEP)ClO_4. [Fe^{III}(*tn*-OEP)]$_2$O (100 mg, 0.06 mmol) was dissolved in 100 mL of dichloromethane, 20% aqueous $HClO_4$ (100 mL) was then added to it, and the resulting mixture was shaken vigorously in a separatory funnel. During that time, the initial greenish solution turned to dark brown. The organic layer was then separated and dried over anhydrous Na_2SO_4. The solution thus obtained was evaporated to dryness to obtain a brown solid, which was then recrystallized using CH_2Cl_2/*n*-hexanes. ***Caution!*** *Perchlorate salts are potentially explosive when heated or shocked. Handle them in milligram quantities with care.* Yield: 42 mg, 75%. Anal. Calcd (found): C, 49.81 (48.87); H, 4.64 (4.69); N, 12.91 (12.88). UV−vis (chloroform) [λ_{max}, nm (ε, M^{-1} cm^{-1})]: 376 (3.5×10^5), 568 (3.6×10^4). EPR data: in solid (77 K), $g_\perp = 5.88$ and $g_\parallel = 2.01$; in toluene (77 K), $g_\perp = 5.90$ and $g_\parallel = 1.99$. ^{1}H NMR ($CDCl_3$, 298 K): CH_2, 40.0; −CH_3, 4.56 ppm. $E_{1/2}(Fe^{3+}/Fe^{2+})$, V (ΔE_p, mV): 0.22 (75).

Fe^{III}(*tn*-OEP)(L)$_2\cdot ClO_4$ and Fe^{II}(*tn*-OEP)(L)$_2$ were prepared using the general procedure; details are given below for one representative case.

Preparation of Fe^{III}(*tn*-OEP)(1-MeIm)$_2\cdot ClO_4$. Fe^{III}(*tn*-OEP)-ClO_4 (50 mg, 0.057 mmol) was dissolved in 3 mL of distilled dichloromethane, 1-MeIm (12 mg, 0.144 mmol) was added to it, and the resulting mixture was stirred for nearly 2 min to form a deep-brown solution. The solution was then filtered quickly to remove any solid residue, and 4 mL of *n*-hexanes was immediately added to the resulting solution and kept for 0.5 h at a constant temperature of 5 °C, during which the solid precipitates out, which was then collected by filtration, washed well with *n*-hexanes, and dried in a vacuum. Yield: 28 mg, 48%. Anal. Calcd (found): C, 51.24 (51.20); H, 5.08 (5.14); N, 16.29 (16.22). UV−vis (benzene) [λ_{max}, nm (ε, M^{-1} cm^{-1})]: 375 (3.12×10^5), 419sh (2.46×10^5), 570 (3.68×10^4). EPR data: in solid (77 K), $g_1 = 1.69$, $g_2 = 2.32$, $g_3 = 2.79$; in toluene (77 K), $g_1 = 1.68$, $g_2 = 2.34$, $g_3 = 2.78$.

Fe^{III}(*tn*-OEP)(4-MeIm)$_2\cdot ClO_4$. Yield: 26 mg, 44%. Anal. Calcd (found): C, 51.22 (51.27); H, 5.08 (5.15); N, 16.28 (16.20). UV−vis (benzene) [λ_{max}, nm (ε, M^{-1} cm^{-1})]: 377 (2.98×10^5), 423sh (2.13×10^5), 646 (1.60×10^4). EPR data: in solid (77 K), $g_1 = 1.68$, $g_2 = 2.28$, $g_3 = 2.83$; in toluene (77 K), $g_1 = 1.69$, $g_2 = 2.31$, $g_3 = 2.80$.

Fe^{III}(*tn*-OEP)(Im)$_2\cdot ClO_4$. Yield: 24 mg, 42%. Anal. Calcd (found): C, 50.28 (50.22); H, 4.82 (4.89); N, 16.75 (16.73). UV−vis (benzene) [λ_{max}, nm (ε, M^{-1} cm^{-1})]: 378 (2.78×10^5), 426sh (1.96×10^5), 645 (1.67×10^4). EPR data: in solid (77 K), $g_1 = 1.67$, $g_2 = 2.27$, $g_3 = 2.84$; in toluene (77 K), $g_1 = 1.68$, $g_2 = 2.29$, $g_3 = 2.82$.

Preparation of Fe^{II}(*tn*-OEP)(1-MeIm)$_2$. Fe^{III}(*tn*-OEP)ClO_4 (25 mg, 0.028 mmol) was dissolved in 10 mL of dichloromethane. 1-MeIm (28 mg, 0.28 mmol) was then added to it, and the resulting mixture was stirred for 1 h. The initial brown solution turned green during the progress of the reaction. The solution was then filtered to remove any solid residue and carefully layered with dry cyclohexane. Upon standing for 7−8 days, a dark-green crystalline solid was formed, which was collected by filtration, washed well with cyclohexane, and dried in a vacuum. Yield: 24 mg, 90%. Anal. Calcd (found): C, 56.68 (56.74); H, 5.62 (5.60); N, 18.02 (18.11). UV−vis (chloroform) [λ_{max}, nm (ε, M^{-1} cm^{-1})]: 372 (2.38×10^5), 412 (2.34×10^5), 576 (2.85×10^4). ^{1}H NMR ($CDCl_3$, 295 K): CH_2, 3.5; −CH_3, 1.24 ppm. $E_{1/2}(Fe^{2+}/Fe^{3+})$, V (ΔE_p, mV): 0.49 (75).

Fe^{II}(*tn*-OEP)(4-MeIm)$_2$. Yield: 23 mg, 85%. Anal. Calcd (found): C, 56.66 (56.61); H, 5.64 (5.71); N, 18.04 (18.09). UV−vis (chloroform) [λ_{max}, nm (ε, M^{-1} cm^{-1})]: 362 (2.78×10^5), 415 (2.74×10^5), 572 (2.25×10^4). ^{1}H NMR ($CDCl_3$, 295 K): CH_2, 3.6; −CH_3, 1.28 ppm. $E_{1/2}(Fe^{2+}/Fe^{3+})$, V (ΔE_p, mV): 0.37 (80).

Fe^{II}(*tn*-OEP)$(Im)_2$. Yield: 21 mg, 82%. Anal. Calcd (found): C, 55.78 (55.71); H, 5.08 (5.00); N, 16.29 (16.35). UV−vis (chloroform) [λ_{max}, nm (ε, M^{-1} cm^{-1})]: 368 (2.64×10^5), 411 (2.58×10^5), 575 (2.62×10^4). ^{1}H NMR ($CDCl_3$, 295 K): CH_2, 3.4; −CH_3, 1.32 ppm. $E_{1/2}(Fe^{2+}/Fe^{3+})$, V (ΔE_p, mV): 0.37 (75).

Instrumentation. UV−vis spectra were recorded on a Perkin-Elmer UV−vis spectrometer. Elemental (C, H, and N) analyses were performed on a CE-440 elemental analyzer. EPR spectra were obtained on a Bruker EMX EPR spectrometer. Cyclic voltammetric studies were performed on a BAS Epsilon electrochemical workstation in dichloromethane with 0.1 M TBAP as the supporting electrolyte; the reference electrode was Ag/AgCl, and the auxiliary electrode was a platinum wire. The concentration of the compounds was on the order of 10^{-3} M. The ferrocene/ferrocenium couple occurs at $E_{1/2} = +0.45$ (65) V vs Ag/AgCl under the same experimental conditions. ^{1}H NMR spectra were recorded on a JEOL 500 MHz instrument. The spectra for paramagnetic molecules were recorded over a 100 kHz bandwidth with 64K data points and a 5 ms 90° pulse. For a typical spectrum, between 2000 and 3000 transients were accumulated with a 50 μs delay time. The residual ^{1}H NMR resonances of the solvents were used as a secondary reference.

X-ray Structure Solution and Refinement. Crystals were coated with light hydrocarbon oil and mounted in the 100 K dinitrogen stream of a Bruker SMART APEX CCD diffractometer equipped with a CRYO Industries low-temperature apparatus, and intensity data were collected using graphite-monochromated Mo Kα radiation (λ = 0.710 73 Å). The data integration and reduction were processed with *SAINT* software.[42] An absorption correction was applied.[43] Structures were solved by direct methods using *SHELXS-97* and were refined on F^2 by a full-matrix least-squares technique using the *SHELXL-97*[44] program package. Non-hydrogen atoms were refined anisotropically. In the refinement, hydrogen atoms were treated as riding atoms using *SHELXL* default parameters. For Fe^{II}(*tn*-OEP)(1-MeIm)$_2$·THF, only the solvent THF is disordered and distributed with two fractional occupancies (with 58 and 42% occupancies). For Fe^{II}(*tn*-OEP)(1-MeIm)$_2$, the methyl groups of two ethyl substituents have disorder in the orientation and split into two fragments. In all cases, the occupancies were originally determined by refinement. The refined occupancies were then fixed in subsequent cycles of refinement.

Computational Details. DFT calculation was carried out by employing a B3LYP hybrid functional using the *Gaussian 03*, revision B.04, package.[40] The method used was Becke's three-parameter hybrid exchange functional,[38] the nonlocal correlation provided by the Lee, Yang, and Parr expression,[39] and the Vosko, Wilk, and Nuair 1980 correlation functional (III) for local correction. The basis set was LANL2DZ for the iron atom and 6-31G** for the carbon, nitrogen, oxygen, and hydrogen atoms. The coordinates were taken directly from the single-crystal X-ray data of Fe^{II}(*tn*-OEP)(1-MeIm)$_2$, and two 1-MeIm ligands were given parallel orientation with respect to each other. Geometry optimization of the molecule was then performed, keeping the spin-state (low-spin) constant. Single-point energy calculation was also performed using DFT for Fe^{III}(*tn*-OEP)(1-MeIm)$_2^+$, in which two axial 1-MeIm ligands were aligned in both parallel and perpendicular orientations separately. The coordinates of the molecule were also generated from the X-ray structure of the corresponding low-spin complex of Fe^{II}(*tn*-OEP)(1-MeIm)$_2$, and 1-MeIm ligands were then rotated manually.

Acknowledgment. We are thankful to the CSIR, India, and the Department of Science and Technology, Government of India, for financial support. R.P., A.C., and S.K.G. thank CSIR, India, for their fellowships. We also thank Dr. Nisanth N. Nair for useful discussion on DFT.

Supporting Information Available: Selected bond distances and angles comparing the geometry-optimized structure and X-ray structures of the molecules (Table S1) and X-ray crystallographic details in CIF format. This material is available free of charge via the Internet at http://pubs.acs.org.

(42) *SAINT+*, 6.02 ed.; Bruker AXS: Madison, WI, **1999**.
(43) Sheldrick, G. M. *SADABS 2.0*; University of Göttingen: Göttingen, Germany, **2000**.
(44) Sheldrick, G. M. *SHELXL-97: Program for Crystal Structure Refinement*; University of Göttingen: Göttingen, Germany, 1997.